Phase Diagram for the Helical Texture in ^{3}He-A*

Dieter Vollhardt,† Y. P. Lin-Liu, and Kazumi Maki

Department of Physics, University of Southern California, Los Angeles, California

The stability region of the helical textures in ^{3}He-A in the v_s–H phase diagram is theoretically determined. Here $\mathbf{v}_s$ is the superflow velocity and $\boldsymbol{H}$ ($\|\mathbf{v}_s$) is the external magnetic field. The pitch of the helix k^{-1} that minimizes the Gibbs free energy and the corresponding inclination angles of $\hat{\boldsymbol{l}}$ and $\hat{\boldsymbol{d}}$ are determined numerically as functions of v_s and H. The NMR frequencies (two longitudinal and four transverse frequencies) associated with the helical texture are obtained.

1. INTRODUCTION

As is well known, a state with superflow in ^{3}He-A is globally unstable in the absence of a magnetic field.[1] However, Bhattacharyya *et al.*[2] have shown that the uniform texture with $\hat{\boldsymbol{l}}\|\mathbf{v}_s$ is locally stable in the dipole-locked case at least in the vicinity of the transition temperature (here $\hat{\boldsymbol{l}}$ is the orbital vector characterizing the ^{3}He-A condensate). We have found recently[3,4] that in the presence of a magnetic field $\mathbf{H}$ parallel to the superflow $\mathbf{v}_s$, the uniform texture transforms into a helical texture across the v_s–H phase boundary that limits the region of the uniform texture $\hat{\boldsymbol{l}}\|\mathbf{v}_s$. Similar suggestions have been made independently by several authors,[5–7] although all of them considered only the dipole-locked case. Very recently Kleinberg[8] has reported the results of zero-sound experiments in superfluid ^{3}He-A in the presence of superflow and magnetic field. Some of his attenuation data (in particular those with small heat current) appear to be consistent with the appearance of the helical texture, although the data for large current do not fit into the picture.

Prior to these developments, it had been demonstrated that a helical texture exists below a certain temperature T_i in the absence of magnetic field.[9–12] More recently Kleinert[12] and Fetter[13] estimated T_i independently. The former obtained $T_i = 0.86\,T_c$, while the latter found $T_i = 0.82\,T_c$, where T_c is the ^{3}He–A transition temperature. Although we do not know the origin

*Work supported by the National Science Foundation under Grant No. DMR 76-21032.

†Present address: Max-Planck-Institut für Physik und Astrophysik, Munich, West Germany.

of this minor discrepancy, their results suggest that the helical texture in the absence of magnetic field is also experimentally accessible.

The object of this paper is first to determine the complete stability region of the helical texture in the v_s–H diagram. We limit ourselves to the Ginzburg–Landau regime for simplicity. We have also assumed that the instability is always associated with the longitudinal fluctuation only. In the vicinity of the phase boundary where the uniform texture with $\hat{l} \| \mathbf{v}_s$ transforms into a helical texture, the above assumption is indeed justified.[4] However, far away from this phase boundary, we cannot exclude the possibility that the instability might be due to a transverse fluctuation. If this is the case, the actual stability region for the helical texture would be smaller than that given in this paper. Furthermore, in the present analysis, we limit ourselves to the helical texture with the lowest Gibbs free energy for given **H** and superflow $\mathbf{v}_s$, although in general there is a finite range of k (inverse of the helical pitch) for which the helical texture is stable.[10] This is partly because the analysis is somewhat simplified in this particular case and party because, in a cylinder or a tube with open ends, this may be the only texture actually realized.[10] Second, we have determined numerically all parameters characterizing the helical texture with the lowest Gibbs free energy.

As already pointed out, we believe that NMR will provide an unambiguous signature of the existence of helical textures. Therefore, we have calculated the resonance frequencies of the helical texture in the whole stability region for a typical $\Omega_A(T)$.

2. THE $\mathbf{v}_s$–H PHASE DIAGRAM

As before,[3,4] we shall consider the ^{3}He-A texture in the presence of both superflow $\mathbf{v}_s$ and magnetic field **H** parallel to each other (say in the z direction). Furthermore, we assume that the texture only depends on z, the direction of the superflow. Then $\hat{l}$ and $\hat{\mathbf{d}}$, describing the orbital and spin components of the condensate, are parametrized as

$$\hat{l} = (\sin\chi\cos\psi, \sin\chi\sin\psi, \cos\chi)$$
$$\hat{\mathbf{d}} = (\sin\theta\cos\phi, \sin\theta\sin\phi, \cos\theta) \tag{1}$$

The free energy density of the system in reduced units is then written as[4]

$$\begin{aligned}\mathcal{G} = &-(1+s)^{-1}p^2 + \frac{1}{2}(3-2s)\chi_z^2 + 2\frac{(1-s)^{1/2}}{1+s}p\psi_z \\ &+ \frac{1}{2}\frac{s(3-s)}{1+s}\psi_z^2 + (1+s)[\theta_z^2 + (\sin^2\theta)\phi_z^2] \\ &+ \{1-[\cos\chi\cos\theta + \sin\chi\sin\theta\cos(\psi-\phi)]^2\} + h^2\cos^2\theta \end{aligned} \tag{2}$$

where $s = \sin^2 \chi$, $p = -s(1-s)^{1/2}\psi_z + (1+s)v_s/v_{s0}$, $h = H/H_0$, and

$$v_{s0}\left[\equiv \frac{\hbar}{2m}\left(\frac{\chi_N \Omega_A^2(T)}{\rho_{s11}(T)}\right)^{1/2}\right] = \frac{\hbar}{(2m)^{1/2}\xi_\perp} \simeq 1 \frac{\text{mm}}{\text{sec}}$$

$$H_0[\equiv \Omega_A(T)(\chi_N/\Delta\chi)^{1/2}] \simeq 20 \text{ Oe} \tag{3}$$

and $\xi_\perp$ is the dipole coherence length.

Here p is the normalized superfluid (mass) current, H is the external magnetic field ($\|\mathbf{v}_s$), $\Omega_A(T)$ is the Leggett frequency, and $\Delta\chi$ is the anisotropic part of the magnetic susceptibility of ^{3}He-A.

In an earlier analysis[4] (LVM), we had determined the boundary between the uniform texture with $\hat{\mathbf{l}} \| \mathbf{v}_s$ and the helical texture by expanding Eq. (2) in powers of χ and θ, the inclination angles of $\hat{\mathbf{l}}$ and $\hat{\mathbf{d}}$ from the z axis. We shall now examine the stability of the helical texture for arbitrary values of χ and θ. For this purpose we first set*

$$\psi_z = \phi_z = k \tag{4}$$

Here we assumed that both $\hat{\mathbf{d}}$ and $\hat{\mathbf{l}}$ form helices with the same pitch. Substituting Eq. (4) into Eq. (2), we obtain

$$\tilde{\mathcal{G}} = \mathcal{G} - \mathcal{G}_{\text{uni}} = \mathcal{G}_0 + 2k\mathcal{G}_1 + k^2\mathcal{G}_2 \tag{5}$$

where

$$\mathcal{G}_0 = \frac{s}{1+s}p^2 + \sin^2(\chi - \theta) - h^2 \sin^2 \theta$$

$$\mathcal{G}_1 = p\left[\frac{(1-s)^{1/2}}{1+s} - 1\right]$$

$$\mathcal{G}_2 = (1+s)\sin^2 \theta + \frac{1}{2}s\frac{3-s}{1+s} \tag{6}$$

Here we have subtracted from $\mathcal{G}$ the free energy density of the uniform texture $\mathcal{G}_{\text{uni}}$ given by

$$\mathcal{G}_{\text{uni}} = p^2 + 2p\psi_z + h^2 \tag{7}$$

The possible solutions with constant χ and θ are then determined by

$$\partial\tilde{\mathcal{G}}/\partial\chi = 0, \qquad \partial\tilde{\mathcal{G}}/\partial\theta = 0 \tag{8}$$

Let us denote a pair of χ and θ thus determined by χ_0 and θ_0. Equation (8) implies that no force is acting on $\hat{\mathbf{l}}$ and $\hat{\mathbf{d}}$ in this particular configuration. Finally, the stability criteria of this helical texture are given in terms of

*A similar analysis is carried out in the dipole-locked case in Ref. 10.

eigenvalues λ_i of the eigenequations

$$\lambda\,\delta\chi = \left(\frac{\partial^2\tilde{\mathcal{G}}}{\partial\chi^2}\right)_0 \delta\chi + \left(\frac{\partial^2\tilde{\mathcal{G}}}{\partial\chi\,\partial\theta}\right)_0 \delta\theta + \left(\frac{\partial^2\tilde{\mathcal{G}}}{\partial\chi\,\partial k}\right)_0 \delta k \tag{9a}$$

$$\lambda\,\delta\theta = \left(\frac{\partial^2\tilde{\mathcal{G}}}{\partial\chi\,\partial\theta}\right)_0 \delta\chi + \left(\frac{\partial^2\tilde{\mathcal{G}}}{\partial\theta^2}\right)_0 \delta\theta + \left(\frac{\partial^2\tilde{\mathcal{G}}}{\partial\theta\,\partial k}\right)_0 \delta k \tag{9b}$$

$$\lambda\,\delta k = \left(\frac{\partial^2\tilde{\mathcal{G}}}{\partial\chi\,\partial k}\right)_0 \delta\chi + \left(\frac{\partial^2\tilde{\mathcal{G}}}{\partial\theta\,\partial k}\right)_0 \delta\theta + \left(\frac{\partial^2\tilde{\mathcal{G}}}{\partial k^2}\right)_0 \delta k \tag{9c}$$

Where $\delta\chi$, $\delta\theta$, and δk are fluctuations of χ, θ, and k, and the subscript 0 on the second derivatives indicates that they are taken at $\chi = \chi_0$ and $\theta = \theta_0$. Then the texture is stable when all of the three eigenvalues λ_1, λ_2, and λ_3 are nonnegative.

In general the above criteria result in a finite range of k for which the helical texture is stable.[10] However, the largest stability region for the helical texture can be obtained by choosing the optimal k at the beginning. Furthermore, in a system with open ends, this helical texture with the optimal k may be most favored, as the corresponding Gibbs free energy is the lowest. Therefore we shall limit ourselves hereafter to the texture with this optimal k. Then we can first eliminate k from Eq. (5) by setting $\partial\tilde{\mathcal{G}}/\partial k = 0$ and obtain

$$\tilde{\mathcal{G}} = \mathcal{G}_0 - (\mathcal{G}_1)^2/\mathcal{G}_2 \tag{10}$$

Now χ_0 and θ_0 are determined numerically from Eq. (8). In this case the stability criteria are given by Eqs. (9a) and (9b) with $\delta k = 0$. In other words $\tilde{\mathcal{G}}$ has a local minimum at $\chi = \chi_0$ and $\theta = \theta_0$ if the corresponding texture is stable. As the parameters p and h are changed, the local minimum at $\chi = \chi_0$ and $\theta = \theta_0$ develops ultimately into a saddle point. At this point the helical texture becomes locally unstable. We have constructed Fig. 1 in this way. In region I the uniform texture with $\hat{\mathbf{l}}\|\hat{\mathbf{d}}\|\mathbf{v}_s$ is stable. Region II designates the region where the helical texture is stable. Drawn into region II are curves of constant k, the wave number of the helix, obtained by the minimization procedure. k increases monotonically with increasing p. Note that in region II, p is always smaller than $(1+s)v_s/v_{s0}$, as the twist of the $\hat{\mathbf{l}}$ vector leads to a negative contribution in the mass current. Ignoring region I, region II has roughly triangular shape because the upper and lower phase boundaries are almost linear for $h \lesssim 0.4$ and the upper boundary is given by $p = 1.13$, while the lower one is given by $p = 2.10h$. Somewhat unusual is the needlelike tip where the stability region terminates. Here the upper and lower boundaries join smoothly at $p = 1.159$ and $h = 0.588$ rather than cross at finite angle. In Fig. 2 we show curves of constant χ_0 and θ_0, the inclinations of $\hat{\mathbf{l}}$ and $\hat{\mathbf{d}}$ from

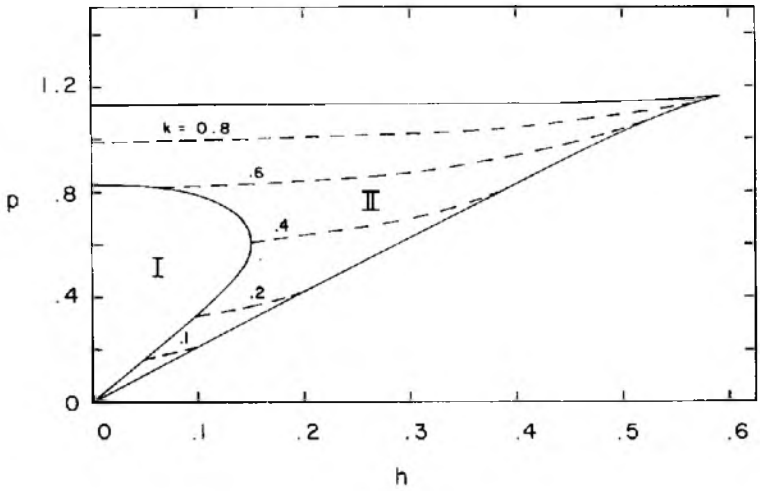

Fig. 1. The stability region (II) of the helical texture, where p is the reduced superflow and h is the reduced magnetic field. In region I the uniform texture with $\hat{\boldsymbol{l}} \| \hat{\mathbf{d}} \| \mathbf{v}_s$ is stable. Broken curves indicate the optimal wave vector k (in units of $\sqrt{2}\xi_{\perp}^{-1}$)associated with the helical texture.

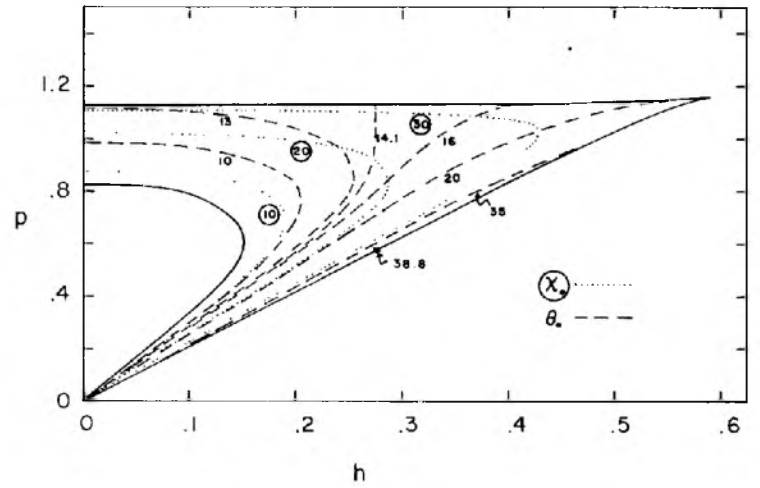

Fig. 2. The tilt angles of $\hat{\boldsymbol{l}}$ (χ_0) and $\hat{\mathbf{d}}$ (θ_0) from the flow direction drawn on phase diagram of the helical texture. Numbers attached to curves are the corresponding angles in degrees.

the z axis in the helical texture. At the boundary between I and II both χ_0 and θ_0 start from zero. In the vicinity of this phase boundary the curves of constant χ_0 and constant θ_0 are very similar because the nuclear dipole energy essentially locks $\hat{\mathbf{l}}$ and $\hat{\mathbf{d}}$ together, so that their relative angle $\chi_0 - \theta_0$ is small and positive; in the helical texture χ_0 is always larger than θ_0. We have already shown[4] that near the phase boundary χ is given by

$$\sin^2 \chi = a(h - h_{\mathrm{I}})/h_{\mathrm{I}} \tag{11}$$

for $h > h_{\mathrm{I}}$, where h_{I} is the reduced magnetic field at the boundary and the coefficient has been calculated along the phase boundary.[4] The present calculation indicates that Eq. (11) is valid throughout the helical region for small p.

At the lower boundary $\chi_0 = 37.8°$ and $\theta_0 = 37.8°$ for $p = h = 0$. As p increases along the lower boundary, χ_0 increases monotonically and at the tip of the triangle it takes the value $\chi = 39.0°$. On the other hand, θ_0 first increases up to 38.8° at $p = 0.3$ and then starts to decrease again, so that $\theta_0 = 25.1°$ at the tip. At the upper boundary χ_0 starts with 35°, while θ_0 starts with 13.1° at $h = 0$. As h increases, both χ_0 and θ_0 increase monotonically and at the triangular tip $\chi_0 = 39°$ and $\theta_0 = 20.8°$. This implies that at the tip χ_0 has a single value independent of how the tip is approached, while θ_0 is multivalued at the tip. This feature is evident from Fig. 2. The anomalous $\hat{\mathbf{d}}$ behavior near the tip is also recognizable in the mode that drives the instability of the helical texture. This mode (the soft mode) is the one with a vanishing eigenvalue of Eq. (9). These eigenmodes are determined numerically. We find that at the upper boundary, the instability is due to a pure $\hat{\mathbf{l}}$ motion for small h. As h is increased, the $\hat{\mathbf{d}}$ vector also begins to be involved in the instability. At the lower boundary, on the other hand, the instability is caused by a joint $\hat{\mathbf{l}}$ and $\hat{\mathbf{d}}$ motion for small h. As h is increased, the $\hat{\mathbf{l}}$-vector fluctuations become less important, so that near the triangular tip, the instability is due to an almost pure $\hat{\mathbf{d}}$ oscillation. On the other side of the tip (the upper boundary), the instability is then due to an $\hat{\mathbf{l}}$–$\hat{\mathbf{d}}$ motion but 180° out of phase.

3. MAGNETIC RESONANCES

An NMR experiment will provide a unique probe of the local conformation of a texture if the texture is not dipole-locked. Since in the helical texture the chiral symmetry along the superflow direction is broken, the transverse resonance frequencies split into two branches of resonances depending on the polarization of a radiofrequency magnetic field. The general expressions necessary to determine the spin wave dispersion have

TABLE I

Parameters Characterizing the Helical Texture for Given p and h

p	h	χ_0	θ_0	k
0.15	0.05	9	8.95	0.089
	0.0625	24	23.91	0.083
0.25	0.0875	13	12.81	0.148
	0.1	21	20.76	0.141
	0.1125	31	30.78	0.131
0.35	0.1125	8	7.74	0.213
	0.1375	20	19.52	0.202
	0.1625	35	34.59	0.177
0.45	0.1375	7	6.60	0.281
	0.1625	16	15.24	0.270
	0.1875	24	23.16	0.255
	0.2125	39	38.38	0.220
0.55	0.15	3	2.72	0.355
	0.175	11	10.07	0.347
	0.2	17	15.77	0.336
	0.225	24	22.63	0.318
	0.25	32	30.80	0.293
0.65	0.15	1	0.86	0.437
	0.1875	10	8.69	0.427
	0.225	17	15.09	0.411
	0.2625	23	20.97	0.389
	0.3	34	32.29	0.345
0.75	0.1375	3	2.38	0.528
	0.1875	10	8.08	0.517
	0.2375	16	13.28	0.500
	0.2875	22	18.96	0.473
	0.35	35	32.61	0.402
0.85	0	6	4.27	0.634
	0.075	7	5.01	0.632
	0.15	11	8.00	0.623
	0.225	16	11.98	0.606
	0.3	21	16.54	0.576
	0.35	26	21.58	0.540
	0.4	36	32.66	0.463
0.95	0	15	9.48	0.744
	0.075	15	9.53	0.742
	0.15	17	10.94	0.735
	0.225	19	12.55	0.722
	0.3	22	15.18	0.699
	0.375	26	19.29	0.656
	0.45	36	31.14	0.541
1.05	0	22	11.72	0.880
	0.075	23	12.22	0.880
	0.15	23	12.43	0.874
	0.225	24	13.26	0.865
	0.3	26	14.81	0.849
	0.375	28	16.89	0.820
	0.45	31	20.74	0.760
	0.5125	39	32.80	0.598

already been obtained[4] for arbitrary χ and θ:

$$(\omega^2 - L_{11}\Omega_A^2)(\omega^2 - \omega_0^2 \sin^2\theta - L_{22}\Omega_A^2) - (\omega\omega_0 - L_{12}\Omega_A^2)^2 \cos^2\theta = 0 \tag{12}$$

where

$$\begin{aligned} L_{11} &= [\sin\chi \cos(\chi - \theta)]/\sin\theta + (1+s)q^2 \\ L_{22} &= (\sin 2\chi)/\sin 2\theta - h^2 \cos 2\theta + (1+s)q^2 \\ L_{12} &= 2(1+s)kq \end{aligned} \tag{13}$$

Here q is the wave vector of the spin wave, $\omega_0 = \gamma H$ is the Larmor frequency, and Ω_A is the Leggett frequency.

We have also shown that the longitudinal rf field couples to the $q = 0$ mode, while the transverse rf field couples to the mode with $q = \pm k$. This leads to two longitudinal resonance frequencies and four transverse resonance frequencies.

Making use of Eq. (12), we have calculated the resonance frequencies of the helical texture in the whole region II. A graphical presentation of the result is somewhat difficult because not only is a single point in the phase diagram associated with six resonance frequencies, but also because all

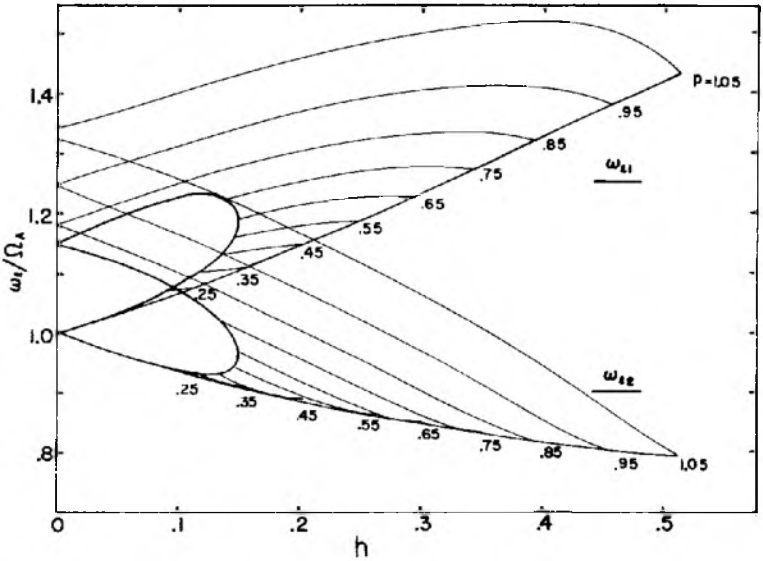

Fig. 3. The longitudinal resonance frequencies ω_l for fixed superflow p as functions of h, the reduced magnetic field at the temperature $T = 0.95T_c$. The numbers on the curves correspond to values of p.

frequencies are temperature dependent due to $\Omega_A(T)$. For convenience therefore we give in Table I the values of χ_0, θ_0, and k for various points (p, h) of the stability region.

These values together with Ω_A completely determine all resonance frequencies. As an example, we shall show a family of resonance frequencies at constant superflow as functions of the reduced external field at one temperature ($T = 0.95 T_c$). The two longitudinal resonance frequencies are shown in Fig. 3. Near the I–II phase boundary, they reduce to the previous result

$$\omega_{l1,2} = (\lambda_l \Omega_A^2 + \tfrac{1}{4}\omega_0^2)^{1/2} \pm \tfrac{1}{2}\omega_0 \tag{14}$$

with $\lambda_l = 1 + k^2 \geq 1$. We thus have one family of curves increasing and the other decreasing with an increasing magnetic field. The lower (heavy) lines indicate the phase boundaries (the upper boundaries are not shown). At the I–II boundary the intensities of ω_{l1} and ω_{l2} vanish. They start linearly with $h - h_1$ for $h > h_1$ in the vicinity of the phase boundary. Figures 4a and 4b show the transverse frequencies ω_{t1}^{+}, ω_{t2}^{+} (which couple to $M_+ = M_x + iM_y$) and ω_{t1}^{-}, ω_{t2}^{-} (which couple to $M_- = M_x - iM_y$), respectively. In the vicinity

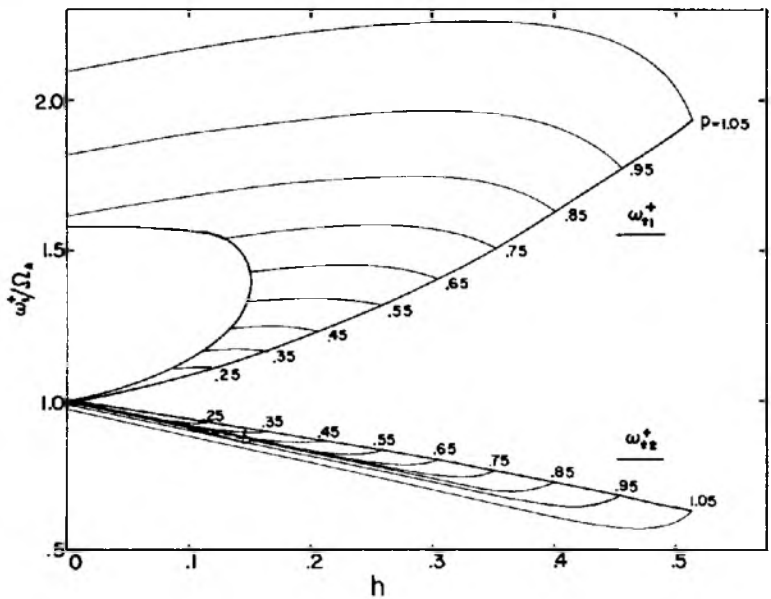

Fig. 4a. The transverse resonance frequencies ω_l^+ (of the modes that couple to M_+) as functions of the reduced field h. The numbers attached to the curves correspond to values of p.

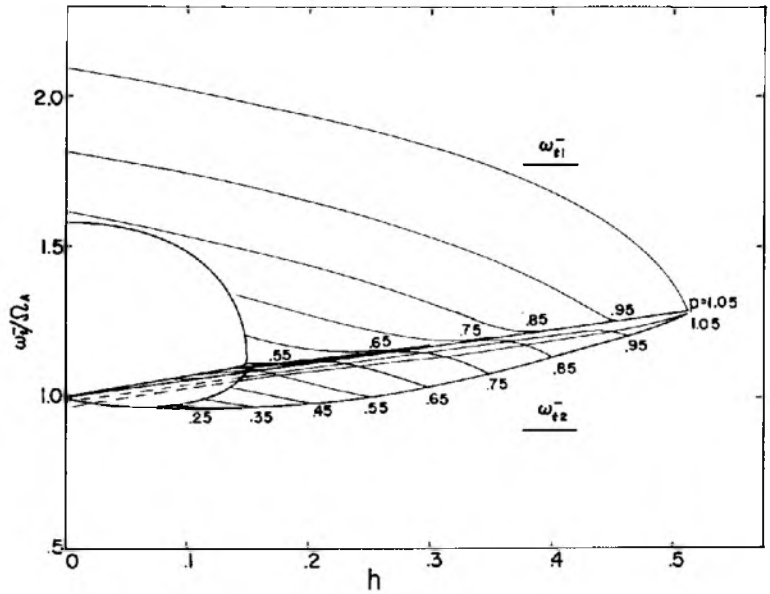

Fig. 4b. The transverse resonance frequencies ω_t^- (of the modes that couple to M_-) as functions of the reduced field h for $T/T_c = 0.95$. The numbers correspond to values of p. In the region of small p and h ($p < 0.55$ and $h < 0.15$) the resonance frequencies are almost degenerate and only depend on h.

of the I–II boundary, they reduce to[4]

$$\omega_{t1}^+ = (\lambda_t \Omega_A^2 + \tfrac{1}{4}\omega_0^2)^{1/2} + \tfrac{1}{2}\omega_0, \qquad \omega_{t2}^+ = (\Omega_A^2 + \tfrac{1}{4}\omega_0^2)^{1/2} - \tfrac{1}{2}\omega_0$$
$$\omega_{t1}^- = (\Omega_A^2 + \tfrac{1}{4}\omega_0^2)^{1/2} + \tfrac{1}{2}\omega_0, \qquad \omega_{t2}^- = (\lambda_t \Omega_A^2 + \tfrac{1}{4}\omega_0^2)^{1/2} - \tfrac{1}{2}\omega_0 \qquad (15)$$

where $\lambda_t = \lambda_l + 3k^2$.

Note that ω_{t1}^- and ω_{t2}^+ are nothing but the bulk resonances of the uniform texture ($\mathbf{v}_s \| \hat{\mathbf{l}} \| \hat{\mathbf{d}}$). In the helical texture the bulk intensities for ω_{t1}^- and ω_{t2}^+ are abruptly split into those for ω_{t1}^+, ω_{t2}^+ and ω_{t1}^- and ω_{t2}^- as the phase boundary is crossed. From Eqs. (15) we see that ω_{t1}^+ increases rapidly with the magnetic field, while ω_{t2}^+ stays almost constant. On the other hand, ω_{t1}^- and ω_{t2}^- appear to intersect each other, because ω_{t1}^- increases with h, while ω_{t2}^- decreases weakly with h. However, these two frequencies repel each other, as seen from Fig. 4b, since these two modes are coupled.

4. CONCLUSION

Limiting ourselves to the Ginzburg–Landau regime ($T \simeq T_c$), we have shown that the helical texture is stable in a rather extended region in the

v_s–H phase diagram, namely in a triangular region formed by $p < 1.16$ (or $v_s \lesssim 1.1$ mm/sec) and $h \lesssim 0.5p$. The largest magnetic field allowed in the helical texture is $h = 0.588$ (or $H \simeq 12$ Oe). In the present analysis the possibility of a transverse instability is ignored, as it is irrelevant, at least in the vicinity of the I–II phase boundary.[4]

In the phase diagram, parameters characterizing the helical texture are determined numerically. In particular, we have determined six NMR frequencies in the helical texture, which should be experimentally accessible.

Yet another way to identify the helical texture would be by means of a zero-sound attenuation experiment. The sound wave couples with the $\hat{l}$ texture. When a sound wave with the wave vector $\mathbf{q}$ is incident with a finite angle to the z axis, there should be jumps in the attenuation coefficient when $q_z = 2k$, just as in the cholesteric liquid crystals,[14] where $\mathbf{k}$ is the wave vector of the helical texture.

ACKNOWLEDGMENT

One of us (DV) gratefully acknowledges a dissertation scholarship by the Studienstiftung des Deutschen Volkes.

REFERENCES

1. G. E. Volovik and V. P. Mineyev, preprint; see also N. D. Mermin, in *Quantum Liquid*, J. Ruvalds and T. Regge, eds. (North-Holland, Amsterdam, 1978).
2. P. Bhattacharyya, T. L. Ho, and N. D. Mermin, *Phys. Rev. Lett.* **39**, 1290 (1977); M. C. Cross and M. Liu, *J. Phys. C* **11**, 1795 (1978).
3. Y. R. Lin-Liu, K. Maki, and D. Vollhardt, *J. Phys. Lett. (Paris)* **39**, 381 (1978).
4. Y. R. Lin-Liu, D. Vollhardt, and K. Maki, *Phys. Rev. B*, in press.
5. S. Takagi, *Prog. Theor. Phys. (Kyoto)* **60**, 934 (1978).
6. W. N. Saslow and C. R. Hu, *J. Phys. Lett. (Paris)* **39**, 379 (1978).
7. J. Hook and H. E. Hall, preprint.
8. R. L. Kleinberg, *Phys. Rev. Lett.* **42**, 182 (1979).
9. A. L. Fetter, *Phys. Rev. Lett.* **40**, 1656 (1978).
10. H. Kleinert, Y. R. Lin-Liu, and K. Maki, *Phys. Lett.* **70A**, 27 (1979).
11. H. Kleinert, *Phys. Lett.* **71A**, 66 (1979).
12. H. Kleinert, Collected Field Theory of Superfluid ^{3}He, Lecture Note (1978).
13. A. L. Fetter, preprint.
14. I. Muscutariu, S. Bhattacharya, and J. B. Ketterson, *Phys. Rev. Lett.* **35**, 1584 (1975).